

Discommensuration-driven superconductivity in the charge density wave phases of transition-metal dichalcogenides

Chuan Chen,^{1,2} Lei Su,³ A. H. Castro Neto,^{1,2} and Vitor M. Pereira^{1,2}

¹*Centre for Advanced 2D Materials and Graphene Research Centre,
National University of Singapore, Singapore 117546*

²*Department of Physics, National University of Singapore, Singapore 117542*

³*Department of Physics, University of Chicago, Chicago, Illinois 60637, USA*
(Dated: March 14, 2022)

We introduce a McMillan-Ginzburg-Landau theory to describe the cooperative coexistence of charge-density and superconducting order in two-dimensional crystals. With a free-energy that explicitly accounts for the competition between commensurate and incommensurate ground states, we are able to map the transition between these phases and monitor the development of discommensurations in the near-commensurate regime. Attributing the enhancement of superconducting order to density-wave fluctuations, we propose a coupling scheme that yields a phase diagram in qualitative agreement with experiments in conducting transition metal dichalcogenides. The model predicts the development of non-uniform superconductivity similar to that arising from a pair-density wave, with a spatial texture driven by the underlying charge-density wave fluctuations.

PACS numbers: 71.10.Hf, 71.45.Lr, 74.20.De

Recent experiments suggest a relation between emergent superconductivity in doped transition-metal dichalcogenides (TMDs) and fluctuations of their charge density wave (CDW) order [1–4]. The archetype example of 1T-TiSe₂ (TiSe₂ in short) displays superconductivity (SC) amidst CDW order as soon as the nature of the latter changes from commensurate (C) to incommensurate (IC) under electron doping [1, 5–7] or pressure [6, 8], either in bulk or 2D samples [1, 9]. SC is limited to a dome over a small range of the external parameter x (doping or pressure) in the T - x phase diagram. Since CDW correlations persist in the SC phase [10] and the dome is centered at the putative quantum critical point of the commensurate CDW (C-CDW) phase, it has been suggested that SC might arise (or be enhanced) as a result of CDW fluctuations [4, 11, 12].

The basic excitation of a C-CDW is called *discommensuration* (DC) [13]: a localized defect (domain wall) where the phase of the order parameter jumps by $2\pi\nu$, with ν the commensurability fraction [13–15]. DCs have been observed in TiSe₂ by STM [2, 3] above the optimal SC transition temperature ($T_{\text{sc}}^{\text{max}} \simeq 4$ K), and are implied by inelastic scattering [7]. This suggests that the CDW converts from C to IC through a near-commensurate (NC) regime characterized by a finite density of DCs, similarly to the cases of 2H-TaSe₂ [13] or 1T-TaS₂ [16].

Although the range $T < T_{\text{sc}}$ remains unexplored by STM, Little-Parks magnetoresistance oscillations [17] observed in TiSe₂ films [1] were interpreted as a result of supercurrents constrained by an underlying periodicity tied to the CDW background. STM observations of enhanced density of states within DCs [2] indirectly support this. Moreover, the onset of a DC network introduces new low-energy phonons [18, 19] that can couple to electrons and induce a Cooper instability [20]. Both

ingredients suggest that the underlying theory must tie SC to both fluctuations and the domain structure of the electronic CDW.

To investigate the potential role of CDW fluctuations in either inducing or enhancing the SC order, we propose an extension of McMillan’s Ginzburg-Landau framework for the CDW in layered TMDs [13, 21]. It incorporates a SC order parameter coupled to the electronic density via DCs. In the vicinity of the C-IC transition (the NC regime), the predicted phase diagram reproduces the experimental one in TiSe₂ with no fine-tuning of parameters (all ~ 1). The nature of the SC phase is interesting and novel: the model implies non-uniformity in the NC regime close to T_{sc} and, with decreasing temperature, SC order might sequentially percolate from 0d to 1d to 2d.

CDW order — McMillan established the approach to the C-IC transition in terms of a free energy functional with a complex order parameter [13, 21]. Although the approach is general, the relevant nonlinear and *umklapp* terms depend on the particular ordering vectors and commensurability condition [21]. To be specific, we consider here the case of TiSe₂ since its small carrier density makes it an easily tuneable system [1, 6, 7]. Both bulk [22] and monolayer [23] TiSe₂ undergo a second order phase transition to the C-CDW phase characterized by the formation of a 2×2 superlattice in the 2d planes. The experimentally measured density modulation $\delta\rho(\mathbf{r})$ is contributed by three plane waves with wavevectors $\mathbf{Q}_j^C \equiv \mathbf{G}_j/2$, where \mathbf{G}_j ($j=1, 2, 3$) are primitive reciprocal vectors related by C_3 rotations [22]. As the in-plane ordering is the same in both bulk and monolayer [23], we neglect the inter-layer coupling and focus on the doping-temperature phase diagram of a TiSe₂ monolayer [1, 7]. We ignore electronic disorder [24], as appropriate for gate-induced doping in encapsulated few-layer sys-

tems [1], or doping by Cu intercalation that donates conduction electrons without visible disruption of the electronic bandstructure [5, 12]. Following the approach of references [21, 25, 26], we define the complex CDW order parameters, $\psi_j(\mathbf{r}) \equiv \varphi_j(\mathbf{r})e^{i\theta_j(\mathbf{r})}$, according to

$$\delta\rho(\mathbf{r}) \equiv \sum_j e^{i\mathbf{r}\cdot\mathbf{Q}_j^C} \psi_j(\mathbf{r}) + \text{c.c.}, \quad (1)$$

where $\psi_j(\mathbf{r})$ encodes deviations from the C state. To describe the IC phase, we introduce the wavevectors \mathbf{Q}_j^I that parametrize a uniform IC-CDW with the same symmetry. In line with experiments [20], we take $\mathbf{Q}_j^I = (1 + \delta)\mathbf{Q}_j^C$, where δ quantifies the incommensurability, and further define $\mathbf{q}_j^I \equiv \mathbf{Q}_j^I - \mathbf{Q}_j^C$, $q^I \equiv |\mathbf{q}_j^I| = \delta|\mathbf{Q}_j^C|$.

The free energy density consists of a conventional Ginzburg-Landau portion,

$$f_0(\mathbf{r}) \equiv A \sum_j |\psi_j|^2 + B \sum_j |(i\nabla_j + \mathbf{q}_j^I) \psi_j|^2 + G \sum_j |\psi_j|^4, \quad (2a)$$

where the B term favors a solution $\psi_j(\mathbf{r}) \propto e^{i\mathbf{q}_j^I \cdot \mathbf{r}}$ that distorts $\delta\rho(\mathbf{r})$ towards an IC state [27]. The quadratic coefficient is assumed to vanish linearly at a critical temperature: $A \equiv t \propto T - T_{\text{icdw}}$, t being the reduced temperature. The presence of non-colinear waves contributing to $\delta\rho(\mathbf{r})$ entails additional terms in the free energy to 4th order [21, 25]. Symmetry dictates them to be [20]

$$f_1(\mathbf{r}) \equiv -\frac{E}{2} \sum_j (\psi_j^2 + \psi_j^{*2}) - \frac{3D}{2} (\psi_1\psi_2\psi_3 + \text{c.c.}) - \frac{M}{2} \sum_j (\psi_j\psi_{j+1}^*\psi_{j+2}^* + \text{c.c.}) + \frac{K}{2} \sum_{i \neq j} |\psi_i\psi_j|^2. \quad (2b)$$

The total CDW free energy reads $\mathcal{F}_{\text{cdw}} \equiv \int [f_0(\mathbf{r}) + f_1(\mathbf{r})] d\mathbf{r}$. The subscript j runs cyclically over $\{1, 2, 3\}$ in all our expressions (e.g., $\psi_5 \equiv \psi_2$). Physically, the last 3 terms in Eq. (2b) reflect the electrostatic cost incurred by the superposition of distinct density waves [28]. The E term represents the *lock-in* energy since it lowers the total energy of a C-CDW but averages out for an IC-CDW, thereby favoring the former.

Eq. (2b) induces harmonics of any IC-CDW characterized by $\psi_j \propto e^{i\mathbf{q}_j \cdot \mathbf{r}}$, implying that the equilibrium IC state consists of a linear combination of all compatible harmonics and making the analytical minimization of \mathcal{F}_{cdw} a formidable task. We tackle the problem numerically with a systematic expansion of the order parameter, as pioneered by Nakanishi *et al.* [26, 29, 30]. The method amounts to expanding each $\psi_j(\mathbf{r})$ in terms of $e^{i\mathbf{q}_j \cdot \mathbf{r}}$ and all the two-dimensional harmonics spawned by the non-linear terms in Eq. (2b) [20]. This converts \mathcal{F}_{cdw} from a functional of $\psi_j(\mathbf{r})$ into a function of a countable set of amplitudes $\Delta_{j;lmn}$ and wavevectors $\mathbf{q}_{j;lmn}$ of the different harmonics. The equilibrium solution follows from minimizing \mathcal{F}_{cdw} with respect to these parameters as well

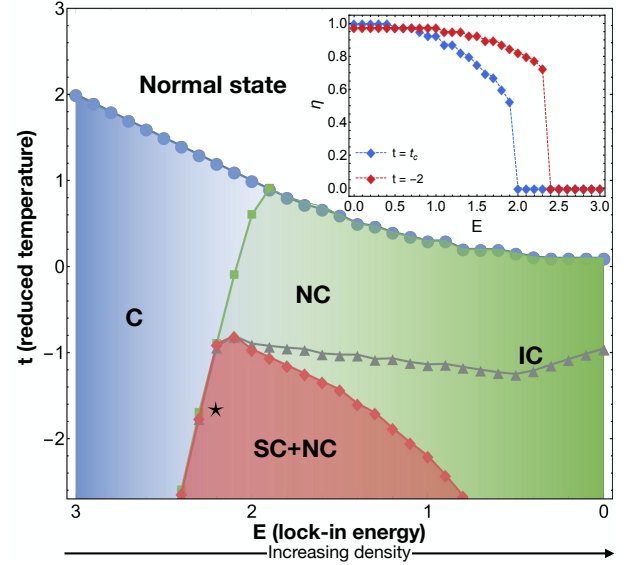


FIG. 1. Phase diagram obtained by minimizing \mathcal{F}_{cdw} . Labels C, NC and IC stand for commensurate, near-commensurate and homogeneously incommensurate CDW phases, respectively. When $\mathcal{F}_{\text{cdw}} < 0$, the system is in a CDW state and the C phase corresponds to $\eta = 0$. The green line represents the C-IC boundary, $E_c(t)$. The red line indicates the boundary of the SC phase including the linear E dependence in the CDW-SC coupling a_s of Eq. (3) ($a_1 = 500E$); it becomes the gray line if a_s is E -independent ($a_1 = 500 \times 2.1$). The inset shows the equilibrium η at t_c (first order transition) and at low temperature.

as \mathbf{q}_j itself. We take $\mathbf{q}_j \parallel \mathbf{q}_j^I$, and introduce $\eta \equiv |\mathbf{q}_j|/q^I$ that determines if the solution is a C-CDW ($\eta = 0$), a uniformly IC-CDW ($\eta = 1$), or in between (NC-CDW).

CDW phase diagram — As we are only interested in scrutinizing the C-IC transition, we map the phase diagram in the E - t plane fixing the remaining parameters to $A = t$, $K = G = 2B(q^I)^2 = -2D = 2M = 2$ [20]. Without any fine tuning, this choice already allows us to concentrate on the C-IC boundary shown in Fig. 1 and drive the transition via E , which controls the energy gain of having a C-CDW. Physically, a *smaller* E can be mapped to *larger* electron densities because: (i) phenomenologically, electron doping reduces the stability of the C state in favor of an IC one [1, 2, 7]; (ii) the lock-in gain reflects the condensation energy of the C-CDW phase in a microscopic description, and the latter has been shown to decrease with doping in the excitonic theory for the C-CDW in TiSe_2 [20, 31–33]. For this reason, the horizontal E axis in the figure is reversed so that electron densities increase from left to right.

The phase diagram in Fig. 1 exhibits the anticipated stability of the C state at large E (low density) and its suppression below a critical, temperature-dependent lock-in parameter: $E_c(t)$. Note that the critical temperature, $t_c(E)$, decreases when progressing from the C to the IC state, in agreement with the experimental trend

[1, 7]. Likewise in agreement is the abrupt loss of the C phase indicated by the steep slope of the line $E_c(t)$. In light of our earlier definition of t , the asymptotic tendency $t_c(E \rightarrow 0) \approx 0$ means that $T_c \rightarrow T_{\text{icdw}}$, or that, as expected from (2a), a uniform IC state is ultimately preferred in the absence of lock-in energy. The inset shows the equilibrium value of η at the critical temperature of the normal-CDW transition and at low temperatures: It grows towards $\eta \approx 1$ with decreasing E , implying that the dominant wavevectors contributing to $\delta\rho(\mathbf{r})$ increasingly approach the reference IC vector \mathbf{Q}_j^I .

Knowledge of η is insufficient to characterize the rich spatial texture of the charge modulation which depends on the detailed harmonic content that minimizes \mathcal{F}_{cdw} (supplementary Eq. S6). Fig. 2(a) shows $\delta\rho(\mathbf{r})$ at the representative point close to the C-CDW boundary marked by \star in Fig. 1. Figs. 2(b,c) show line cuts of the phase and amplitude of the order parameters $\psi_j(\mathbf{r}) \equiv \varphi_j(\mathbf{r})e^{i\theta_j(\mathbf{r})}$ along the vertical dashed line in panel (a). The phase $\theta_j(\mathbf{r})$ displays a stepwise variation with periodic slips of π . Since (1) implies that regions where $\theta_j(\mathbf{r}) \approx 0 \bmod \pi$ are commensurate with the Bravais lattice, the spatial profile of the phase reveals an equilibrium state characterized by domains of approximately C-CDW separated by DCs of π . This NC regime replicates the characteristics of CDW domain walls investigated by STM slightly above T_{sc} in TiSe_2 [2, 3].

Adapting Eq. (2b) to a general commensurability condition $\mathbf{Q}^C = \nu \mathbf{G}$ with ν a rational number ($\nu = 1/2$ for TiSe_2), one obtains a corresponding domain structure with phase steps of $2\pi\nu$ across domain boundaries [14, 18, 25, 26, 30]. In 1d phase-only reductions of this problem [$\varphi_j(\mathbf{r}) = \text{const.}$], the saddle-point condition for \mathcal{F}_{cdw} becomes a sine-Gordon equation [14, 18] and DCs correspond to its soliton solutions. Even though our problem of interest is two-dimensional, Eq. (1) still consists of a linear combination of 1d CDW modulations along each \mathbf{G}_j . It is thus not surprising that each $\theta_j(\mathbf{r})$ in Fig. 2(b) retains a soliton-like nature.

The DCs form a 2D Kagome superlattice overlaying the C-CDW, as highlighted by the yellow-dashed contours in Fig. 2(a). For a general commensurability fraction ν , the period of the DC network is $L = 2\pi\nu/(\eta q^I) = \sqrt{3}a/(\eta\delta)$, where a is the lattice constant of the crystal in the normal phase.

Note that the amplitude of $\psi_i(\mathbf{r})$ is also significantly modulated: Fig. 2(c) shows it can drop more than 30% at each DC. The high variational freedom possible in our harmonic expansion permits the CDW to distort in order to minimize both the lock-in and gradient terms of \mathcal{F}_{cdw} . The solution thus acquires both C and IC features, consisting of domains with nearly flat phase and high amplitude (C-CDW), joined by domain boundaries where the amplitude drops to lessen the cost in deviating from commensurability, and the phase jumps so that, on

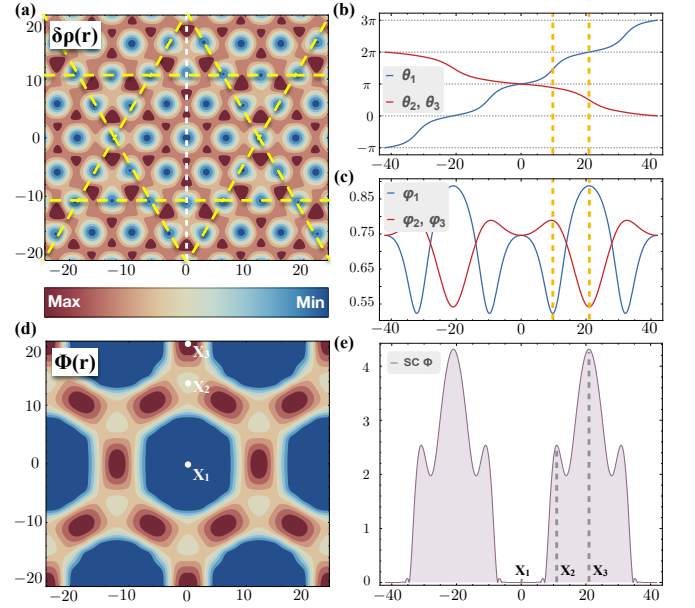


FIG. 2. (a) Real space plot of the density profile $\delta\rho(\mathbf{r})$ at $E=2.2$, $t=-1.7$ (in units of $\sqrt{3}a/2\pi$, with a the lattice constant). The yellow-dashed lines mark the places where the phase of each CDW order parameter, $\psi_j(\mathbf{r})$, jumps by π . (b) and (c) respectively show the phase and amplitude of $\psi_j(\mathbf{r})$ along the white vertical cut marked in (a). (d) The SC order parameter, $\Phi(\mathbf{r})$, in the same region as (a). (e) $\Phi(\mathbf{r})$ along the vertical cut marked in (a).

spatial average, $\langle\theta_j(\mathbf{r})\rangle \approx \mathbf{q}_j^I \cdot \mathbf{r}$ (IC-CDW).

Coupling to superconductivity — It is natural to expect these DCs to couple strongly with the SC order parameter: On the one hand, the development of a DC superlattice as in Fig. 2(a) introduces new low energy phonons [18–20] that might enhance any intrinsic phonon-mediated pairing tendency. On the other hand, DCs are but CDW fluctuations. While both phase and amplitude fluctuations are gapped in the C regime [15], the transition to the NC state releases them to potentially favor SC through fluctuation-induced pairing.

As a minimal approach to describe the interplay between the two orders, we propose extending the conventional [34] Ginzburg-Landau free energy associated with the SC order parameter, $\Phi(\mathbf{r})$, by writing

$$\mathcal{F}_{\text{sc}} \equiv \int \left[a_s(T, \nabla\psi_j) |\Phi|^2 + b_s |\nabla\Phi|^2 + c_s |\Phi|^4 \right] d\mathbf{r}. \quad (3)$$

Making a_s a function of $\nabla\psi_j$ permits the enhancement of SC by deviations from a C-CDW. To lowest order in the interaction and inhomogeneity, a_s should have the form $a_s = a_0 - a_1 \sum_j |\nabla\psi_j|^2$, where a_0 is the conventional quadratic coefficient ($a_0 \propto T - T_0$ if there are sources of pairing other than CDW fluctuations, which could lead to SC below some temperature T_0) and $a_1 > 0$ so that SC is stabilized within regions of fluctuating C order (we take a_1 to be T -independent). This captures, phenomenolog-

ically, fluctuation-induced ($a_0 = \text{const.}$) and fluctuation-enhanced ($a_0 \propto T - T_{\text{sc}}$) pairing, as well as the spatial enhancement of the electronic DOS at DCs [2].

The total free energy is now $\mathcal{F} = \mathcal{F}_{\text{cdw}} + \mathcal{F}_{\text{sc}}$ and the coupling in (3) requires a self-consistent solution for both $\psi_j(\mathbf{r})$ and $\Phi(\mathbf{r})$. As in TiSe_2 $T_{\text{cdw}} \simeq 60 \text{ K}$ and $T_{\text{sc}} \simeq 4 \text{ K} \ll T_{\text{cdw}}$ [1, 5, 7, 8], the CDW is already well developed when SC emerges. This justifies solving the two problems independently, where \mathcal{F}_{sc} is minimized subject to a passive CDW background $\psi_j(\mathbf{r})$ determined by \mathcal{F}_{cdw} . (Although we note that the back-influence of a finite $\Phi(r)$ on $\psi_j(r)$ implied by Eq. (3) increases CDW fluctuations via DCs so that SC and DCs mutually stabilize each other.) A representative result [20] is shown in Fig. 2(d) for the CDW solution in panel (a) [35]. The most significant feature is the non-uniformity of $\Phi(\mathbf{r})$ that follows the spatial texture of the DC network. The section plotted in Fig. 2(e) shows there is no SC within the C domains [$\Phi(\mathbf{x}_1) = 0$] but only at and near the DCs, and that SC is reinforced when two DCs overlap at the vertices of the Kagome: $\Phi(\mathbf{x}_3) \approx 2\Phi(\mathbf{x}_2)$.

Interestingly, it is clear from how $\nabla\psi_j$ enters the quadratic coefficient a_s in Eq. (3) that the development of SC in the NC regime can take place in three stages with decreasing temperature: (i) it begins at $T_{\text{sc}}^{0\text{d}}$ with the nucleation of isolated SC dots at the Kagome vertices, as illustrated at the top of Fig. 3(a) that depicts a unit cell of the DC/SC superlattice; (ii) at $T_{\text{sc}}^{1\text{d}} \lesssim T_{\text{sc}}^{0\text{d}}$ the dots have grown and overlap to percolate the system in a connected network as in Fig. 2(d); (iii) ultimately, at $T_{\text{sc}}^{2\text{d}} \lesssim T_{\text{sc}}^{1\text{d}}$ the whole system becomes superconducting. (The SC boundaries in the phase diagram correspond to $T_{\text{sc}}^{0\text{d}}$.) The coupling proposed in Eq. (3) therefore predicts that, depending on the temperature, the SC order can have either a 0d, 1d or 2d character. This can be directly probed with temperature-dependent local spectroscopy across the SC transition. In the absence of other pairing mechanisms, this picture predicts that if the penetration length of $\Phi(\mathbf{r})$ into the C region is smaller than L , it is possible to have $T_{\text{sc}}^{2\text{d}} = 0$ in the NC region of the phase diagram. SC would then span the system, at most, through the 1d network defined by the DCs.

The area of SC stability in the phase diagram depends on whether the parameter a_1 in Eq. (3) varies with E . If it does not, SC persists from the NC to the IC limit at temperatures below the gray line in Fig. 1. It remains in the IC limit because $|\nabla\psi_j|$ is finite, thereby supporting uniform SC. In the specific case of doped TiSe_2 , however, SC exists only in a dome-shaped portion of the phase diagram, over a finite density range [1, 5]. This phenomenology can be captured by replacing $a_1 \rightarrow a_1 E$ in the parameter a_s , making it depend both implicitly (through ψ_j) and explicitly on the lock-in parameter E . This amounts to making the coupling to CDW fluctuations weaker at higher densities, which is physically plausible in view of screening. The SC boundary numerically recalculated in

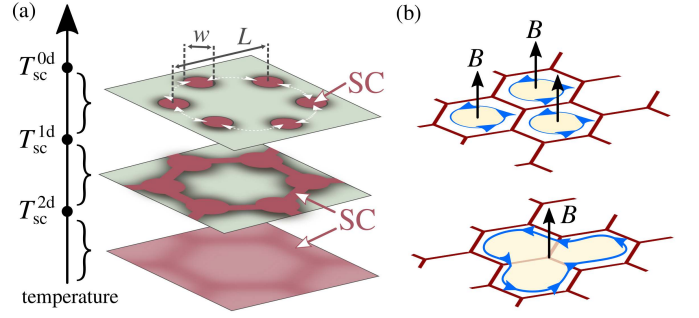


FIG. 3. (a) Schematic of the distinct non-uniform SC regimes spatially correlated with the DC network: nucleation and expansion of the SC order parameter ($T_{\text{sc}}^{1\text{d}} < T \leq T_{\text{sc}}^{0\text{d}}$), percolation ($T_{\text{sc}}^{2\text{d}} < T \leq T_{\text{sc}}^{1\text{d}}$), and finite everywhere. See supplementary Fig. S4 for actually calculated textures. (b) Illustration of how the connectivity in the percolation regime constrains the vortex structure, with impact in the magnetic response.

this way drops to lower temperature when $E \rightarrow 0$, as conveyed by the red line in Fig. 1, which qualitatively reproduces the experimental SC dome (see also Fig. S3).

Ramifications — The feasibility of non-uniform percolative SC in the NC regime is determined by the characteristic width of DCs (w), their separation L (the size of C domains), and the SC coherence length ξ ($\sim 12 \text{ nm}$ in TiSe_2 [36]). Likely, $w \lesssim \xi$, not sufficient to permit fully developed SC grains in the range $T_{\text{sc}}^{1\text{d}} < T < T_{\text{sc}}^{0\text{d}}$ where the model predicts nucleation at the vertices of the DC network.

The situation in the range $T_{\text{sc}}^{2\text{d}} < T < T_{\text{sc}}^{1\text{d}}$ has interesting implications in the presence of a magnetic field, B . First, vortices are naturally pinned by the DC lattice, even in the absence of disorder, and their motion correlated. Second, given the likelihood that $w \lesssim \xi$, vortices would not squeeze within DCs; the supercurrent would instead circulate along a linked network of 1D SC channels [34], as illustrated in Fig. 3(b). If $L \gg \xi$, we may regard this as a microscopic version of SC wire grids [37–45], a distinctive feature of which are oscillatory dips as a function of B in thermodynamic [37] and transport [39] properties, with period determined by rational fractions ($f = \phi/\phi_0$) of the flux through the grid's elementary plaquette ($\phi \sim BL^2$, $\phi_0 \equiv h/2e$) [43, 44, 46].

It is tempting to speculate whether such non-uniform SC texture can underlie the Little-Parks oscillations found in the SC phase of TiSe_2 near optimum doping [1]. To test it, assume the grid is hexagonal as in Fig. 2(d) ($f = 1/4$ [44]) and take the first experimental magnetoresistance dip at $B \simeq 0.13 \text{ T}$. With our results, we obtain the incommensurability factor $\delta \sim 0.01$ and a typical distance between DCs $L \sim 70 \text{ nm}$ [47]. Compellingly, x-ray diffraction does reveal $\delta \sim 5\text{--}15\%$ in the superconducting dome [7], and STM finds DCs separated by 10's of nm at optimum doping above T_{sc} [2]. It is noteworthy how

these estimates agree with experiments.

Our model captures qualitatively well the emergence of SC correlated with the suppression of the C-CDW. This phenomenology is not unique to TiSe_2 , but documented across a number of $2H$ and $1T$ TMDs [4] spanning both good metals and semimetals, as well as distinct commensurability conditions. Our approach straightforwardly extends to those cases [20], providing a definite and universal phenomenological foundation to further explore the interplay between these two coexisting orders and their fluctuations.

VMP was supported by the Ministry of Education of Singapore through grant MOE2015-T2-2-059 and AHCN by the National Research Foundation of Singapore under its Medium-Sized Centre Programme. Numerical computations were carried out at the HPC facilities of the NUS Centre for Advanced 2D Materials.

-
- [1] L. J. Li, E. C. T. O'Farrell, K. P. Loh, G. Eda, B. Özyilmaz, and A. H. Castro Neto, *Nature* **529**, 185 EP (2015).
 - [2] S. Yan, D. Iaia, E. Morosan, E. Fradkin, P. Abbamonte, and V. Madhavan, *Phys. Rev. Lett.* **118**, 106405 (2017).
 - [3] A. M. Novello, M. Spera, A. Scarfato, A. Ubaldini, E. Giannini, D. R. Bowler, and C. Renner, *Phys. Rev. Lett.* **118**, 017002 (2017).
 - [4] B. Wang, Y. Liu, K. Ishigaki, K. Matsubayashi, J. Cheng, W. Lu, Y. Sun, and Y. Uwatoko, *Phys. Rev. B* **95**, 220501 (2017).
 - [5] E. Morosan, H. W. Zandbergen, B. S. Dennis, J. W. G. Bos, Y. Onose, T. Klimczuk, A. P. Ramirez, N. P. Ong, and R. J. Cava, *Nat. Phys.* **2**, 544 (2006).
 - [6] Y. I. Joe, X. M. Chen, P. Ghaemi, K. D. Finkelstein, G. a. de la Peña, Y. Gan, J. C. T. Lee, S. Yuan, J. Geck, G. J. MacDougall, T. C. Chiang, S. L. Cooper, E. Fradkin, and P. Abbamonte, *Nat. Phys.* **10**, 421 (2014), 1309.4051.
 - [7] A. Kogar, G. A. de la Peña, S. Lee, Y. Fang, S. X.-L. Sun, D. B. Lioi, G. Karapetrov, K. D. Finkelstein, J. P. C. Ruff, P. Abbamonte, and S. Rosenkranz, *Phys. Rev. Lett.* **118**, 027002 (2017).
 - [8] A. F. Kusmartseva, B. Sipos, H. Berger, L. Forró, and E. Tutiš, *Phys. Rev. Lett.* **103**, 236401 (2009).
 - [9] L. Li, C. Chen, K. Watanabe, T. Taniguchi, Y. Zheng, Z. Xu, V. M. Pereira, K. P. Loh, and A. H. C. Neto, arXiv:1803.10936 (2018), 1803.10936.
 - [10] M. Spera, A. Scarfato, E. Giannini, and C. Renner, arXiv (2017), 1710.04096.
 - [11] H. Barath, M. Kim, J. F. Karpus, S. L. Cooper, P. Abbamonte, E. Fradkin, E. Morosan, and R. J. Cava, *Phys. Rev. Lett.* **100**, 106402 (2008).
 - [12] C. Chen, B. Singh, H. Lin, and V. M. Pereira, *Phys. Rev. Lett.* **121**, 226602 (2018).
 - [13] W. L. McMillan, *Phys. Rev. B* **14**, 1496 (1976).
 - [14] P. Bak and V. J. Emery, *Phys. Rev. Lett.* **36**, 978 (1976).
 - [15] G. Grüner, *Density Waves in Solids* (Addison-Wesley, 1994).
 - [16] R. E. Thomson, B. Burk, A. Zettl, and J. Clarke, *Phys. Rev. B* **49**, 16899 (1994).
 - [17] W. A. Little and R. D. Parks, *Phys. Rev. Lett.* **9**, 9 (1962).
 - [18] W. L. McMillan, *Phys. Rev. B* **16**, 4655 (1977).
 - [19] K. Nakanishi and H. Shiba, *J. Phys. Soc. Japan* **45**, 1147 (1978).
 - [20] See Supplemental Material at [URL will be inserted by publisher], which includes references [1–3, 6, 7, 12–14, 18–21, 23, 25, 26, 29–34, 48–54].
 - [21] W. L. McMillan, *Phys. Rev. B* **12**, 1187 (1975).
 - [22] F. J. Di Salvo, D. E. Moncton, and J. V. Waszczak, *Phys. Rev. B* **14**, 4321 (1976).
 - [23] P. Chen, Y.-H. Chan, X.-Y. Fang, Y. Zhang, M.-Y. Chou, S.-K. Mo, Z. Hussain, A.-V. Fedorov, and T.-C. Chiang, *Nat. Commun.* **6**, 8943 (2015).
 - [24] Disorder can introduce additional effects not seen in the experimental cases we consider, see [55, 56].
 - [25] A. E. Jacobs and M. B. Walker, *Phys. Rev. B* **21**, 4132 (1980).
 - [26] K. Nakanishi and H. Shiba, *J. Phys. Soc. Jpn.* **43**, 1839 (1977).
 - [27] The actual magnitude of \mathbf{q}_j^I does not play a role in the subsequent energy minimization because it can be absorbed into the definition of B .
 - [28] The form of interactions between density waves here is specific to the case of TiSe_2 .
 - [29] K. Nakanishi, H. Takater, Y. Yamada, and H. Shiba, *J. Phys. Soc. Jpn.* **43**, 1509 (1977).
 - [30] K. Nakanishi and H. Shiba, *J. Phys. Soc. Jpn.* **44**, 1465 (1978).
 - [31] P. A. Lee, T. M. Rice, and P. W. Anderson, *Solid State Commun.* **14**, 703 (1974).
 - [32] A. Kotani, *J. Phys. Soc. Jpn.* **42**, 408 (1977).
 - [33] A. Kotani, *J. Phys. Soc. Jpn.* **42**, 416 (1977).
 - [34] M. Tinkham, *Introduction to Superconductivity: Second Edition* (McGraw Hill, Inc., New York, 1996).
 - [35] The SC boundary in Fig. 1 was obtained with $a_0 = 10t + 60$ and $b_s = c_s = 1$.
 - [36] E. Morosan, L. Li, N. P. Ong, and R. J. Cava, *Phys. Rev. B* **75**, 104505 (2007).
 - [37] B. Pannetier, J. Chaussy, R. Rammal, and J. C. Villegier, *Phys. Rev. Lett.* **53**, 1845 (1984).
 - [38] H. D. Hallen, R. Seshadri, A. M. Chang, R. E. Miller, L. N. Pfeiffer, K. W. West, C. A. Murray, and H. F. Hess, *Phys. Rev. Lett.* **71**, 3007 (1993).
 - [39] X. S. Ling, H. J. Lezec, M. J. Higgins, J. S. Tsai, J. Fujita, H. Numata, Y. Nakamura, Y. Ochiai, C. Tang, P. M. Chaikin, and S. Bhattacharya, *Phys. Rev. Lett.* **76**, 2989 (1996).
 - [40] M. D. Stewart, A. Yin, J. M. Xu, and J. M. Valles, *Science* **318**, 1273 (2007).
 - [41] S. Teitel and C. Jayaprakash, *Phys. Rev. Lett.* **51**, 1999 (1983).
 - [42] S. Alexander, *Phys. Rev. B* **27**, 1541 (1983).
 - [43] Q. Niu and F. Nori, *Phys. Rev. B* **39**, 2134 (1989).
 - [44] Y.-L. Lin and F. Nori, *Phys. Rev. B* **65**, 214504 (2002).
 - [45] J. Berger and J. Rubinstein, *Connectivity and superconductivity*, Vol. 62 (Springer Science & Business Media, 2001).
 - [46] K. Park and D. A. Huse, *Phys. Rev. B* **64**, 134522 (2001).
 - [47] Since $a = 0.35 \text{ nm}$ for TiSe_2 and $\eta \sim 1$ (Fig. 1), we have $L = \sqrt{3}a/(\eta\delta) = [\phi_0/(2\sqrt{3}B)]^{1/2} \simeq 70 \text{ nm}$ and $\delta \sim 0.01$.
 - [48] S. A. Jackson, P. A. Lee, and T. M. Rice, *Phys. Rev. B* **17**, 3611 (1978).

- [49] M. Leroux, I. Errea, M. Le Tacon, S.-M. Souliou, G. Garbarino, L. Cario, A. Bosak, F. Mauri, M. Calandra, and P. Rodière, *Phys. Rev. B* **92**, 140303 (2015).
- [50] D. B. McWhan, R. M. Fleming, D. E. Moncton, and F. J. DiSalvo, *Phys. Rev. Lett.* **45**, 269 (1980).
- [51] D. E. Moncton, J. D. Axe, and F. J. Disalvo, *Phys. Rev. Lett.* **34**, 734 (1975).
- [52] C. Monney, E. F. Schwier, M. G. Garnier, N. Mariotti, C. Didiot, H. Cercellier, J. Marcus, H. Berger, A. N. Titov, H. Beck, and P. Aebi, *New J. Phys.* **12**, 125019 (2010).
- [53] A. H. Castro Neto, *Phys. Rev. Lett.* **86**, 4382 (2001).
- [54] B. Sipos, A. F. Kusmartseva, A. Akrap, H. Berger, L. Forró, and E. Tutiš, *Nat. Mater.* **7**, 960 (2008).
- [55] J. S. Chen, J. K. Wang, S. V. Carr, S. C. Vogel, O. Gourdon, P. Dai, and E. Morosan, *Phys. Rev. B* **91**, 045125 (2015).
- [56] A. Banerjee, A. Garg, and A. Ghosal, *Phys. Rev. B* **98**, 104206 (2018).

SUPPLEMENTARY MATERIAL

Discommensuration-driven superconductivity in the charge density wave phases of transition-metal dichalcogenides

Chuan Chen,^{1,2} Lei Su,³ A. H. Castro Neto,^{1,2} and Vitor M. Pereira^{1,2}

¹*Centre for Advanced 2D Materials and Graphene Research Centre,
National University of Singapore, Singapore 117546*

²*Department of Physics, National University of Singapore, Singapore 117542*

³*Department of Physics, University of Chicago, Chicago, Illinois 60637, USA*

CONTENTS

S1. General applicability of the approach to TMDs	3
S2. Transformation of the order parameter under symmetries of the system	5
S3. Free energy derived from the symmetries of the system	6
S4. The commensurate and incommensurate wavevectors in TiSe_2	6
S5. Choice of the CDW free-energy parameters	7
S6. Mapping the lock-in energy to doping	10
S7. Harmonic expansion	11
S7.A. Outline of the method	11
S7.B. Explicit form of the harmonic-expanded free energy	13
S8. Solving for the equilibrium CDW order parameter	14
S9. Explicit form of the SC free energies	16
S10. On the coupling between superconductivity and CDW fluctuations	17
S11. Choice of the superconducting free energy parameters	18
S12. Solving for the equilibrium superconducting order parameter	19
S13. Real-space superconducting order	20
References	22

S1. GENERAL APPLICABILITY OF THE APPROACH TO TMDS

It is important to highlight that the proposal discussed here to phenomenologically couple CDW and superconducting (SC) order is not specific or limited to TiSe_2 . This means, for example, that our framework and qualitative outcome in terms of the correlation between superconductivity and the NC regime does not hinge in any way on a specific choice of \mathbf{Q}_j^I and \mathbf{Q}_j^C , including their relative orientation.

In particular, note that the qualitatively most important contribution in this work is the concept that CDW fluctuations in the NC regime are either the driving mechanism of the superconducting pairing or, at least, are a significant factor in enhancing any underlying pairing (in the sense of BCS via electron-phonon). This is materialized in the proposed SC free energy (\mathcal{F}_{sc} , Eq. 3 of the main text), where the SC order parameter is directly coupled to the fluctuations of the CDW order which, in this Ginzburg-Landau approach, are manifest as DCs. Our presentation of this and the associated parameterization of \mathcal{F}_{sc} make clear that there is nothing specific to TiSe_2 . On the other hand, in order to have a specific connection with experiments and to demonstrate the power and completeness of this approach to describe qualitatively accurate phase diagrams, we have to make a specific choice. Such a choice turns out to be unavoidable in order to extract a phase diagram for the CDW order because the form of the interaction terms in the CDW free energy (Eqs. 2a and 2b) depends explicitly on the type of (in)commensurability condition. In our opinion, the best representative system is indeed TiSe_2 , for the reasons stated in the main text: relatively high CDW and SC transition temperatures, reduced semi-metallic carrier densities that allow one to map the whole CDW and SC phase diagram as a function of doping, and its gate tunability in thin-film samples that allows full mapping of the temperature-density phase diagram using the same sample. This makes TiSe_2 arguably the currently best candidate to investigate the nature of the CDW/SC interplay, and also to validate or constrain our theory.

Notwithstanding, the fact that one must specify a particular (in)commensurability in order to generate a phase diagram does not detract from the general applicability of the approach described here because:

1. For example, if one intends to apply it to the case of 2H-TaSe_2 , one needs only to re-write $f_2(\mathbf{r})$ in Eq. (2b) in the form appropriate to describe a 3×3 CDW, which has in fact been done by a number of authors in the past (for the CDW only)¹⁻³.
2. The fact that the CDW transition between the commensurate and incommensurate phases

takes place via an intermediate NC regime, as explicitly obtained here, is a universal aspect of this transition, irrespective of the commensurability conditions^{3,4}. Therefore, the existence of localized DCs in the NC regime is a universal feature, and so are its implications for the nucleation of the SC order.

3. The above two points associate the appearance of superconductivity in experiments on closely related TMDs with the loss of commensurability of the background charge density wave. Our coupling scheme generates this outcome naturally because the superconducting order parameter is favoured in principle in near-commensurate and IC-CDW regimes where $\nabla\psi_j \neq 0$. This is actually verified by the behavior of other representative layered transition metal dichalcogenides, which are effectively two-dimensional from the electronic point of view. Consider, for example, the well known cases of NbSe₂ and TaSe₂,⁵ or TaS₂⁶:

- (a) Under normal conditions (ambient pressure, undoped) 2H-NbSe₂ undergoes a transition to an IC CDW phase at $T_{\text{icdw}} = 33$ K, which is followed by the onset of superconductivity at $T_{\text{sc}} = 7.2$ K. No commensurate CDW phase is known to exist. The superconducting order appears and coexists within the ICDW state⁷.
- (b) 2H-TaSe₂, on the other hand, has an ICDW transition at $T_{\text{icdw}} = 120$ K, followed by a second transition to a commensurate CDW at $T_{\text{cdw}} = 90$ K⁸. However, this system has not been found to superconduct at any temperature which, within our scheme, is attributed to the fact the underlying CDW is commensurate.
- (c) 1T-TaS₂ has no superconductivity at ambient pressure and displays a commensurate CDW down to zero temperature. Under pressure, the commensurability is suppressed and superconductivity emerges in the near-commensurate regime. The phase diagram is qualitatively similar to that of TiSe₂ (see Fig. 3 of reference 6).

These examples indicate a systematic *anti*-correlation between CDW commensurability and superconductivity, as can be also appreciated in Fig. 1 of reference 9, that compares the experimental T_{cdw} with T_{sc} for a representative set of these compounds.

These observations agree with the qualitative phase diagram predicted in our paper, namely:

- (i) SC is not stabilized in the CCDW state because it would need to energetically compete with it;
- (ii) systems that remain in the near-commensurate or IC-CDW state down to low temperatures eventually develop superconductivity. For example, unlike TiSe₂ and TaS₂ that have low carrier

density, NbSe₂ is an intrinsically good metal with high carrier density, and hence difficult to dope. Our model explains its experimental behavior upon lowering the temperature in a natural way: NbSe₂ is representative of a system with small lock-in energy sitting towards the right-hand side of our diagram and, consequently, goes first from the normal to an ICDW state, and afterwards becomes superconductor at low temperatures.

S2. TRANSFORMATION OF THE ORDER PARAMETER UNDER SYMMETRIES OF THE SYSTEM

In order to establish a Ginzburg-Landau free energy, we begin with considering the symmetries of the system. Monolayer TiSe₂ has four types of symmetry: translational, C_3 rotation, mirror (along ΓM 's) and inversion. Using the fact that the commensurate wavevectors are $\mathbf{Q}_j^C \equiv \mathbf{G}_j/2$, where \mathbf{G}_j ($j=1,2,3$) are primitive reciprocal vectors related by 120 degree rotations, the order parameters transform as follows.

1. Under translation by a Bravais lattice vector,

$$\begin{aligned}
\delta\rho'(\mathbf{r}) &= \delta\rho(\mathbf{r} - \mathbf{R}_{b,l}) \\
&= \sum_j e^{i\frac{\mathbf{G}_j}{2} \cdot (\mathbf{r} - \mathbf{R}_{b,l})} \psi_j(\mathbf{r} - \mathbf{R}_{b,l}) + c.c \\
&= \sum_j e^{i\frac{\mathbf{G}_j}{2} \cdot \mathbf{r}} e^{-i\frac{\mathbf{G}_j}{2} \cdot \mathbf{R}_{b,l}} \psi_j(\mathbf{r} - \mathbf{R}_{b,l}) + c.c \\
\psi'_j(\mathbf{r}) &= e^{-i\frac{\mathbf{G}_j}{2} \cdot \mathbf{R}_{b,l}} \psi_j(\mathbf{r} - \mathbf{R}_{b,l})
\end{aligned} \tag{S1}$$

2. Under a C_3 rotation,

$$\begin{aligned}
\delta\rho'(\mathbf{r}) &= \delta\rho(C_3^{-1}\mathbf{r}) \\
&= \sum_j e^{i\frac{\mathbf{G}_j}{2} \cdot (C_3^{-1}\mathbf{r})} \psi_j(C_3^{-1}\mathbf{r}) + c.c \\
&= \sum_j e^{i\frac{\mathbf{G}_{j-1}}{2} \cdot \mathbf{r}} \psi_j(C_3^{-1}\mathbf{r}) + c.c \\
&= \sum_j e^{i\frac{\mathbf{G}_j}{2} \cdot \mathbf{r}} \psi_{j+1}(C_3^{-1}\mathbf{r}) + c.c \\
\psi'_j(\mathbf{r}) &= \psi_{j+1}(C_3^{-1}\mathbf{r})
\end{aligned} \tag{S2}$$

3. Under a mirror operation,

$$\begin{aligned}\psi'_1(x, y) &= \psi_1(-x, y) \\ \psi'_2(x, y) &= \psi_3(-x, y) \\ \psi'_3(x, y) &= \psi_2(-x, y)\end{aligned}\tag{S3}$$

4. Under an inversion, \mathcal{I} ,

$$\psi'_j(\mathbf{r}) = \psi_j^*(-\mathbf{r})\tag{S4}$$

S3. FREE ENERGY DERIVED FROM THE SYMMETRIES OF THE SYSTEM

After taking into account the symmetry of the system in the spirit of references 3 and 10, assuming that higher order terms do not play a significant role, and only focusing on the simplest types of coupling which can capture the *lock-in* effect of the commensurate charge density wave (described by the E -term) and the interaction between the three density waves, one arrives at the free energy in Eq. (2):

$$\begin{aligned}f(x) = & A \sum_j |\psi_j|^2 + B \sum_j \left| \left(i \frac{\partial}{\partial x_{\parallel,j}} + \mathbf{q}_j^I \right) \psi_j \right|^2 + C \sum_j \left| \frac{\partial}{\partial x_{\perp,j}} \psi_j \right|^2 - \frac{3D}{2} (\psi_1 \psi_2 \psi_3 + \psi_1^* \psi_2^* \psi_3^*) \\ & - \frac{E}{2} \sum_j (\psi_j^2 + \psi_j^{*2}) + G \sum_j |\psi_j|^4 + \frac{K}{2} \sum_{i \neq j} |\psi_i \psi_j|^2 - \frac{M}{2} \sum_j (\psi_j \psi_{j+1}^* \psi_{j+2}^* + c.c)\end{aligned}\tag{S5}$$

In view of the C_6 rotational symmetry of the CDW and given that we are not interested in the development of other CDW phases due to induced anisotropy, strain, or disorder, we make the gradient term isotropic by choosing $B = C$.

S4. THE COMMENSURATE AND INCOMMENSURATE WAVEVECTORS IN TISE₂

As far as inelastic scattering is concerned, X-ray experiments in Cu-doped bulk samples by Joe *et al.*¹¹ and Kogar *et al.*¹², indicate that, while the incommensurability in the out-of-plane (stacking) direction is detectable experimentally beyond the critical doping, in-plane incommensurabilities were estimated to have too small a coherence length to be observable. Thus, inelastic scattering experiments in doped bulk crystals can only resolve an in-plane charge modulation with the commensurate \mathbf{Q}^C .

It should be stressed, however, that in a system that remains in the near-commensurate (NC) regime, the wavevector \mathbf{Q}^I is only an abstract parameter in the theory, because the system never displays a uniform CDW with this wavevector. Instead, it remains locally commensurate with domain walls. As far as we can tell among all experiments in doped TiSe_2 , this system is indeed either in the strictly commensurate or NC regime depending on the electronic density (these are limited to a maximum doping of less than 0.1 electrons per formula unit, either by the solubility limit in intercalated bulk samples, or by the gate capacitance in back-gate-tuned few-layer samples). Consequently, it is not surprising that bulk probes do not see CDW order with in-plane wavevector \mathbf{Q}^I , but only \mathbf{Q}^C , including in the NC regime. But, as we point out in our introduction, local probes (STM) do see DCs in the CDW phase at optimum SC doping, at temperatures above the SC dome, which favors the view that the system is in the NC-CDW regime when superconductivity emerges.

Transport signatures in ion-gel gated two-dimensional TiSe_2 indirectly suggest the presence of such domain-walls¹³. Subsequent STM experiments have directly shown the presence of intra-layer CDW DCs on surfaces of Cu-doped TiSe_2 ^{14,15}. In the latter case, the DCs lines are perpendicular to the commensurate wavevector \mathbf{Q}^C , which implies that $\mathbf{Q}^I \parallel \mathbf{Q}^C$ is the correct choice in the model.

S5. CHOICE OF THE CDW FREE-ENERGY PARAMETERS

Unlike a conventional Ginzburg-Landau theory for isotropic superconductors that requires only the specification of two independent phenomenological parameters (namely the gap and coherence length), the minimal free energy in Eqs. (2) necessary to reproduce the C / NC / IC-CDW transitions depends on a large number of parameters. This follows from the underlying physics because, even though we are not breaking the system's underlying C_3 rotational symmetry, the presence of three non-colinear density waves and their interactions dictates that one should consider all the terms in Eqs. (2). Therefore, an analysis of the full parameter space, in addition to being a formidable and unwieldy task, would only obfuscate the essential physics.

In addition to temperature (T), the experimental probes of the phase diagram are either doping (x) or pressure, but only the first is applicable to probing the intra-layer CDW order and superconductivity that we are considering here. We thus concentrate on the temperature–doping experimental phase diagrams, and analyze the predictions of our model in terms of variations of these two experimental parameters.

Temperature enters, as usual in a Ginzburg-Landau approach, linearly in the coefficient A of $|\psi_j(\mathbf{r})|^2$,

$$A \equiv t \propto T - T_{\text{icdw}}. \quad (\text{S6})$$

By setting $A = t$ we are defining the energy units of the CDW free energy in terms of the reduced temperature, t , which has a direct relation to the experimental temperatures. As we explain in the main text, the largest influence of electron doping is expected to be in the lock-in energy which is controlled by the term proportional to the parameter E in Eq. (2b). Hence, E and t become the parameters of interest in the theory to map into the experimental x and T , respectively.

The above still leaves the parameters B , G , D , M and K unspecified in the CDW free energy, which require further consideration to determine the appropriate “slice” (t , E) to focus on for comparison with experiments within the whole multidimensional parameter space. In the absence, at the moment, of finer microscopic details from experiments regarding the near-commensurate regime and the large-scale distribution of discommensurations in TiSe_2 , our main consideration is to avoid biasing the final solution towards a particular configuration. We therefore treat all terms in \mathcal{F}_{cdw} on equal footing by proceeding as follows.

1. Since we are mapping experimental changes in temperature and density to $A \equiv t$ and E , and since the various experimental phases are not fragile but consistently reproduced across different samples, as well as bulk and monolayers, these two parameters play the physically more dominant role in the phase diagram. For this reason, and given that the CDW transition occurs at $t \sim 0$, we explore the phase diagram in the region where E is of the order of 1.
2. The parameter B in Eq. (2a) sets the energy cost in deviating the charge modulation from the reference ICDW. In our approach to minimize the CDW free energy, the order parameter $\psi_j(\mathbf{r})$ is expanded in an harmonic series containing a variational wavevector \mathbf{q}_j and all the harmonics thereof induced by the nonlinear terms in the free energy of Eq. (2) (see the details in supplementary section S7 below). Furthermore, recalling that: (i) $\mathbf{Q}_j^C \parallel \mathbf{G}_j$, (ii) that we are experimentally motivated to set $\mathbf{Q}_j^I \parallel \mathbf{Q}_j^C$ (see supplementary section S4) as well as to put $|\mathbf{Q}_1^I| = |\mathbf{Q}_2^I| = |\mathbf{Q}_3^I|$ to narrow the already large variational parameter space (also detailed in supplementary section S7), (iii) and recalling also the definition $\mathbf{q}_j^I \equiv \mathbf{Q}_j^I - \mathbf{Q}_j^C$, we have that $|\mathbf{q}_{1,2,3}^I| = q^I$, which is constant. Therefore, the second term in the free energy density $f_0(\mathbf{r})$ can be re-cast with the magnitude of \mathbf{q}_j^I factored out as follows:

$$B (q^I)^2 \sum_j \left| \left(\frac{i \nabla_j^I}{q^I} + \frac{\mathbf{G}_j}{|\mathbf{G}_j|} \right) \psi_j(\mathbf{r}) \right|^2, \quad (\text{S7})$$

where the summand is now dimensionless. By setting the overall factor $B(q^I)^2 = 1$, we make this contribution to the free energy of the same order as the other terms.

3. We choose $M = -D$ to balance the two different types of phase relation between non-collinear waves. To see this, assume for a moment that all three density waves have the same amplitude, $\psi_j = \varphi e^{i\theta_j}$. The two terms in the free energy proportional to M and D become then:

$$-\frac{3D}{2} \cos(\theta_1 + \theta_2 + \theta_3) - \frac{M}{2} [\cos(\theta_1 - \theta_2 - \theta_3) + \cos(\theta_2 - \theta_3 - \theta_1) + \cos(\theta_3 - \theta_1 - \theta_2)],$$

The lock-in (E) term favors θ_i 's locked to multiples of π , i.e., $\theta_1 = m\pi, \theta_2 = n\pi, \theta_3 = l\pi$ with $m, n, l \in \mathbb{Z}$. By choosing $M = -D$, the D -term favors $m + n + l = 2k + 1$ ($k \in \mathbb{Z}$), while the M -term favors $m + n + l = 2p$ ($p \in \mathbb{Z}$). Since they have similar order of magnitude, both types of phase configuration can appear in real space.

This illustrates that the role of the free energy terms governed by the parameters M and D is to define how the three non-collinear waves interlock their phases in real space or, equivalently, the DCs along each of the three directions. Our choice leads to the Kagome pattern highlighted with the dashed lines in Fig. 2(a). Different choices, such as having M and D with the same sign and/or different magnitudes, translate into different periodic patterns of the DC network in real space. The important thing is that this affects only the precise arrangement of the DC network, and not the fact that there is a DC network. This means that changing the relative sign of M and D or their relative magnitudes (within reasonable bounds, see below) does not change the qualitative nature of the phase diagram. And, most importantly, it does not compromise the nucleation of the superconducting phase to the DCs that we describe in the main text (here too, different choices of these parameters lead only to different spatial profiles of the non-uniform SC order parameter, but not its suppression).

4. Numerical experimentation showed that the sequence of C-NC-IC transitions can be generated as shown in Fig. 1 by setting the magnitude of $B(q^I)^2$, G , D , M and K to 1, without qualitative changes in the features of the diagram (the phases stabilized, the sequence and order of transitions, overall topology of the phase diagram) within a comfortable range of variation in the magnitude of the parameters. We therefore settled on the final choice stated in the main text:

$$A = t, \quad K = G = 2M = -2D = 2, \quad B(q^I)^2 = 1. \quad (\text{S8})$$

Note that all the parameters in the CDW free energy are thus of the same order of magnitude, with no particular one significantly larger or smaller than the others. In other words, there is no fine-tuning of parameters in order to capture a qualitatively correct phase diagram. This can be regarded as a result of building the free energy on well grounded physical considerations. Moreover, having all parameters of the order ~ 1 indicates that: (i) the phases and features shown in Fig. 1 are robust, (ii) the phase diagram shown Fig. 1 is not constrained *a priori* in any way to fit the experimental one.

Finally, and for completeness, we note that the magnitude of our parameters (~ 1) is similar to that found by Nakanishi and Shiba in their earlier work that pioneered the systematic use of the harmonic expansion for the CDW order parameter in the context of 1T and 2H transition metal dichalcogenides^{1,16}. As described in Supplementary Section “Harmonic Expansion”, our treatment of the CDW order parameter consists of an implementation of their method, with the adaptation of including explicitly the harmonic component $\Delta_{j;0}$ to capture the C-CDW in the same expansion. Their work already establishes, across different materials, that the interesting transitions among the C, NC, and IC phases can be analyzed with all parameters ~ 1 .

S6. MAPPING THE LOCK-IN ENERGY TO DOPING

In the section “CDW phase diagram” of the main text we state the following: “*Physically, a smaller E can be mapped to larger electron densities because: (i) phenomenologically, electron doping reduces the stability of the C state in favor of an IC-CDW^{12,13,15}; (ii) the lock-in gain reflects the condensation energy of the C-CDW phase in a microscopic description, and the latter has been shown to decrease with doping in the excitonic theory for the C-CDW in TiSe_2 ^{17–20}*”. Below we elaborate on each of these statements in more detail.

“(i) phenomenologically, electron doping reduces the stability of the C state in favor of an IC-CDW” — This is a purely phenomenological consideration independent of any additional knowledge of the microscopic interactions that stabilize the commensurate CDW phase. It simply states that, in our model, E is the parameter that, when reduced, weakens the stability of the commensurate phase in favor of a NC or incommensurate situation; experimentally, doping weakens the commensurate CDW; therefore, it is natural and reasonable to associate a decreasing E with increased electronic density, on purely phenomenological grounds.

“(ii) the phenomenological lock-in gain reflects the condensation energy of the C-CDW phase in a microscopic description, and the latter has been shown to decrease with doping in the excitonic

theory for the C-CDW in TiSe_2 — In a microscopic description of the C-CDW transition (irrespective of whether it is driven by electron-phonon or electron-electron interactions), the gain in electronic energy (the so-called condensation energy at $T = 0$) is determined by the magnitude of the gap introduced in the bandstructure by the commensurate modulation of electronic density. In the microscopic formulation, the gap is the order parameter. On the other hand, in a Ginzburg-Landau model such as ours, the condensation energy is determined by E . This relationship between the lock-in parameter in the phenomenological treatment and the microscopic condensation energy is essentially the same in the CDW problem as in the Ginzburg-Landau approach to superconductivity. For the CDW case, it is discussed in detail, for example, in G. Grüner’s textbook cited in the main text (see, in particular, section 7.1; see also references 17–19).

The essential point here is that there is a solid microscopic relationship between these two quantities, irrespective of the details of the model or target system. Now, in addition, in TiSe_2 the CDW gap decreases with doping. If this was simply a statement based on the experimental phase diagram, it would not be an independent argument. However, we also know from the specific microscopic calculations reported in reference 21 that the CDW gap/order parameter indeed decreases with doping. Therefore, there is a direct microscopic justification to map the decrease in E with an increase in electron density, entirely at the theoretical level, independently of the experimental observations.

S7. HARMONIC EXPANSION

S7.A. Outline of the method

When we consider an IC-CDW characterized by a certain \mathbf{q}_j , the various terms in Eq. (2b) induce higher harmonics of it. Hence, the equilibrium IC state must consist of a linear combination of infinite compatible harmonics. This fact must be explicitly accounted for in order to properly describe: the C-IC transition, the fact that the equilibrium \mathbf{q}_j changes with temperature, as well as the order of the phase transitions^{5,22}. In addition, despite the insight provided by phase-only models^{4,23}, both the phase and amplitude of the order parameter should be considered to properly describe the stable CDW as, not a uniform plane wave solution, but a wave periodically distorted in real space to accommodate the competing E and B terms in the free energy^{3,22,24}. These two aspects, combined with the fact that the saddle-point equations are nonlinear, make the analytical minimization of $f_{\text{cdw}}(\mathbf{r})$ a formidable problem, except in simplified cases^{3,24}.

A pragmatic approach consists in making a systematic harmonic expansion of the order parameter and minimizing the free energy numerically, as pioneered by Nakanishi *et al.*^{1,16,25}. Accordingly, we consider the expansion

$$\psi_j(\mathbf{r}) = \Delta_{j;0} + \sum_{\substack{0 \leq l,m,n \leq N \\ l \cdot m \cdot n = 0}} \Delta_{j;lmn} \exp(i\mathbf{q}_{j;lmn} \cdot \mathbf{r}), \quad (\text{S9})$$

where $\mathbf{q}_{j;lmn} \equiv (2l+1)\mathbf{q}_j + 2m\mathbf{q}_{j+1} + 2n\mathbf{q}_{j+2}$ are the harmonics of \mathbf{q}_j generated by $f_1(\mathbf{r})$ and l, m, n are positive integers smaller than a cutoff N . Eq. (S9) captures both the C ($\Delta_{j;lmn} = 0$) and an arbitrary IC wave ($\mathbf{q}_{j;lmn} \neq 0$ and $\Delta_{j;lmn} \neq 0$) modulated in amplitude and phase. Although $\{\Delta_{j;0}, \Delta_{j;lmn}\} \in \mathbb{C}$ in general, we make the simplifying assumptions $\Delta_{j;0} \equiv \Delta_0 \in \mathbb{R}$, $\Delta_{j;lmn} \equiv \Delta_{lmn} \in \mathbb{R}$, $\mathbf{q}_j \parallel \mathbf{q}_j^I$, and $|\mathbf{q}_j| \equiv \eta q^I$, which are all compatible with the experimental density modulation $\delta\rho(\mathbf{r})$. Under these conditions, the free energy functional becomes a function of real parameters [a total of $(N+1)^3 - N^3 + 2$],

$$\mathcal{F}_{\text{cdw}}[\eta, \Delta_0, \Delta_{lmn}] \equiv \int [f_0(\mathbf{r}) + f_1(\mathbf{r})] d\mathbf{r}, \quad (\text{S10})$$

where $\Delta_0, \Delta_{lmn}, \eta$, are determined to minimize \mathcal{F}_{cdw} (the explicit form of \mathcal{F}_{cdw} is given below).

We performed the multidimensional minimization of \mathcal{F}_{cdw} numerically with respect to Δ_0 and Δ_{lmn} at fixed η , subsequently scanning the latter in a fixed range. As Eq. (2) penalize deviations of \mathbf{q}_j from \mathbf{q}_j^I (via the B term) and from 0 (via the E term), it is sufficient to scan the range $\eta \in [0, 1]$ to obtain the global minimum. We verified that the expansion (S9) converges rapidly (cf. Fig. S2), and used the quite sufficient cutoff $N = 3$ in all subsequent calculations.

S7.B. Explicit form of the harmonic-expanded free energy

Substituting the order parameter given by Eq. (S9) into Eq. (2) and after some algebra, the free energy can be shown to be equal to:

$$\begin{aligned}
\mathcal{F}_{\text{cdw}}/3 = & \sum_{\substack{l,m,n \geq 0 \\ l \cdot m \cdot n = 0}} \sum_i \left[A + B(\mathbf{q}_{i;lmn} - \mathbf{q}_i^I) \cdot (\mathbf{q}_{i;l'm'n'} - \mathbf{q}_i^I) + 2 \left(G + \frac{K}{2} \right) |\Delta_0|^2 \right] \\
& \times \Delta_{i;lmn} \Delta_{i;l'm'n'}^* \delta(l - l', m - m', n - n') \\
& - \frac{E}{2} \sum_i [\Delta_{i;lmn} \Delta_{i;l'm'n'} \delta(l + l' + 1, m + m', n + n') + c.c.] \\
& - \frac{3D}{2} [\Delta_{1;lmn} \Delta_{2;l'm'n'} \Delta_{3;l''m''n''} \delta(l + n' + m'', m + l' + n'', n + m' + l'') + c.c.] \\
& - \frac{M}{2} \sum_i [\Delta_{i;lmn} \Delta_{i+1;l'm'n'}^* \Delta_{i+2;l''m''n''}^* \delta(l - n' - m'' + 1, m - l' - n'', n - m' - l'') + c.c.] \\
& + G \sum_i \Delta_{i;lmn} \Delta_{i;l'm'n'}^* \Delta_{i;l''m''n''} \Delta_{i;l'''m'''n'''}^* \delta(l - l' + l'' - l''', m - m' + m'' - m''', n - n' + n'' - n''') \\
& + \frac{K}{2} \sum_{i \neq j} \Delta_{i;lmn} \Delta_{i;l'm'n'}^* \Delta_{j;l''m''n''} \Delta_{j;l'''m'''n'''}^* \delta(l - l' + m'' - m''', m - m' + n'' - n''', n - n' + l'' - l''') \\
& + \sum_i \left(A + B(q_i^I)^2 - E \right) |\Delta_{i;0}|^2 + \left(G + \frac{K}{2} \right) |\Delta_{i;0}|^4.
\end{aligned} \tag{S11}$$

Here, the δ -function is defined as

$$\delta(l, m, n) = \begin{cases} 1, & l = m = n, \\ 0, & \text{otherwise.} \end{cases} \tag{S12}$$

In principle, complex $\Delta_{j;lmn}$'s should be used, however, as mentioned in the main text, we studied the case when $\Delta_{j;0} = \Delta_0$, $\Delta_{j;lmn} = \Delta_{lmn}$ and are real. Under these assumptions, the free energy expansion simplifies to:

$$\begin{aligned}
\mathcal{F}_{\text{cdw}}/3 = & + \left(A + \tilde{B} - E \right) \Delta_0^2 + \left(G + \frac{K}{2} \Delta_0^4 \right) + \sum_{\substack{l,m,n \geq 0 \\ l \cdot m \cdot n = 0}} \left[A + \tilde{B} \tilde{\mathbf{q}}_{lmn}^2 + 2 \left(G + \frac{K}{2} \right) |\Delta_0|^2 \right] \Delta_{lmn} \Delta_{lmn} \\
& - E \Delta_{lmn} \Delta_{l'm'n'} \delta(l + l' + 1, m + m', n + n') \\
& - D \Delta_{lmn} \Delta_{l'm'n'} \Delta_{l''m''n''} \delta(l + n' + m'', m + l' + n'', n + m' + l'') \\
& - M \Delta_{lmn} \Delta_{l'm'n'} \Delta_{l''m''n''} \delta(l - n' - m'' + 1, m - l' - n'', n - m' - l'') \\
& + G \Delta_{lmn} \Delta_{l'm'n'} \Delta_{l''m''n''} \Delta_{l'''m'''n'''} \delta(l - l' + l'' - l''', m - m' + m'' - m''', n - n' + n'' - n''') \\
& + K \Delta_{lmn} \Delta_{l'm'n'} \Delta_{l''m''n''} \Delta_{l'''m'''n'''} \delta(l - l' + m'' - m''', m - m' + n'' - n''', n - n' + l'' - l''')
\end{aligned} \tag{S13}$$

where $\tilde{\mathbf{q}}_{lmn}^2 = 4\eta^2[(l^2 + m^2 + n^2) - (lm + ln + mn)] + 2(2l - m - n)\eta(\eta - 1) + (\eta - 1)^2$, with $\eta = |\mathbf{q}_j|/q^I$, notice that the $(q^I)^2$ has been absorbed into $\tilde{B} = B(q^I)^2$.

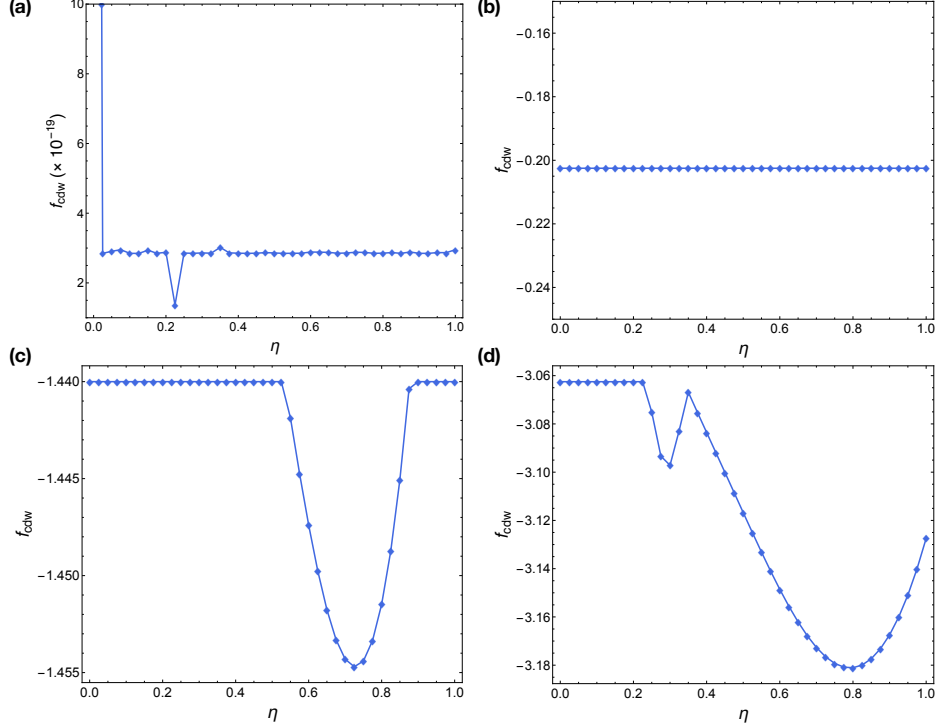


FIG. S1. Minimum of the CDW free energy (in arbitrary units) with respect to η at $E = 2.2$. (a) For $t = 1.2$, the minimum free energy is numerically zero for all η (note the extremely magnified vertical scale to emphasize the threshold of numerical accuracy), indicating a normal state. (b) At $t = 0.3$, the minimum of free energy is independent of η and negative. Only the harmonic amplitude Δ_0 is finite (not shown), which defines a C-CDW state. (c-d) For $t = -1.2$ and $t = -2.3$, the minimum free energy is obtained at a finite η , which implies an I-CDW state.

S8. SOLVING FOR THE EQUILIBRIUM CDW ORDER PARAMETER

Once all the parameters of the CDW free energy are set, to find the absolute minimum of the free energy defined above, we begin by fixing η and obtaining the saddle points in the multidimensional space spanned by the real parameters Δ_0 and Δ_{lmn} . The saddle points are determined by numerically solving the Euler-Lagrangian equations for Δ 's. The result of this step is a curve of the minimum free energy as a function of η , $\mathcal{F}_{\text{cdw}}^{\text{min}}(\eta)$, examples of which are shown in Fig. S1 for different effective temperatures.

The calculations require setting an harmonic cutoff N that restricts the expansion to terms with $0 \leq l, m, n \leq N$. The number of variational parameters is then given by $(N + 1)^3 - N^3 + 2$, which takes into account the constraint that at least one of l, m, n must be zero ($l \cdot m \cdot n = 0$), and includes Δ_0 and η . The convergence of the harmonic expansion is relatively fast and we verified

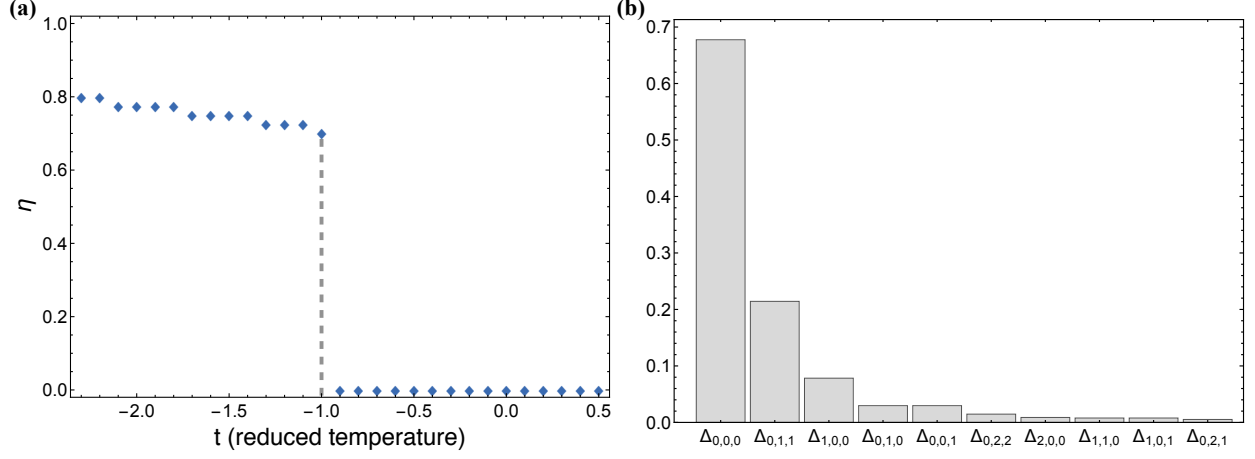


FIG. S2. Results from numerical minimization of free energy. (a) Plot of η versus t at a $E = 2.2$. The jump at $t \approx -1$ indicates a first order nature of the C-IC phase transition. (b) The ten largest Δ 's at $(E, t) = (2.2, -1.7)$. Since $\Delta_{0,0,0}$ is the largest, the CDW phase is not commensurate at this point in the phase diagram.

that $N=3$ yields a good compromise without affecting the accuracy of the results in the range of parameters studied. A typical example of the rapid decay of the higher harmonics is shown in Fig. S2(b).

Since we are minimizing numerically a 39-dimensional function, in order to reduce the chance of finding just a local minimum, we stochastically repeat each minimization multiple times (typically 200 repetitions) feeding random initial values to the minimization routine and extract the absolute minimum. Moreover, we verified that the same results are obtained with independent implementations of the minimization procedure in Mathematica and Matlab which use different algorithms for absolute minimization.

The equilibrium state is identified by the harmonic content of the order parameter for the value of η that yields the absolute minimum of the free energy, as illustrated in Fig. S1. There are three possible outcomes: (i) If $\mathcal{F}_{\text{cdw}}^{\min}(\eta) = 0$ as in Fig. S1(a), the equilibrium corresponds to the normal state, without either CCDW or ICDW. (ii) If $\mathcal{F}_{\text{cdw}}^{\min}(\eta) \leq 0$ but constant with η as in Fig. S1(b), we have a CCDW state [which is always confirmed by inspecting that Δ_0 is the only non-zero component of $\psi(\mathbf{r})$]. (iii) Otherwise, $\mathcal{F}_{\text{cdw}}^{\min}(\eta)$ will have a global minimum at a given η , as in the cases shown in Fig. S1(c) and Fig. S1(d), which indicates that the equilibrium state is an ICDW. As can be seen from Fig. S2(a), due to the finite jump of η at the transition temperature, the C-IC transition is of first order.

S9. EXPLICIT FORM OF THE SC FREE ENERGIES

As described in the main text, we considered two explicit forms of the Ginzburg-Landau free energy for the SC amplitude $\Phi(\mathbf{r})$ that differ only in whether the constant that couples it to the CDW order parameter depends on the lock-in energy E . In the first form the free energy in Eq. (3) reads explicitly

$$\mathcal{F}_{\text{sc}} = \int \left[\left(a_0 - a_1 \sum_j |\nabla \psi_j|^2 \right) |\Phi|^2 + b_s |\nabla \Phi|^2 + c_s |\Phi|^4 \right] d\mathbf{r}, \quad (\text{S14})$$

where the constants were chosen as follows: $a_0 \equiv T = 10t + 60$, where t represents the reduced temperature, $t = (T - T_{\text{icdw}})/10$, here we have used the fact that $T_{\text{icdw}} \approx 60$ K from the X-ray experiment¹². In addition, the gray SC boundary in Fig. 1 was obtained by using $a_1 = 500 \times 2.1$ so that the maximum T_{sc} in this calculation matches the one obtained on the basis of Eq. (S15) at the calculated tip of the SC dome; $b_s = c_s = 1$ for simplicity since, presently, we are interested only in the qualitative characteristics of the solution and its relation to the DC network, and not in the specific details of how stiff the SC order parameter is, which is controlled by b_s , but regarding which no experimental evidence or data exists yet.

Since all constants are independent of E in this scheme, the effect of the lock-in energy enters only indirectly via the dependence of the CDW texture on E . Using this free energy and these parameters, the SC transition occurs at the gray line shown in the phase diagram of Fig. 1.

The second scheme discussed in the main text makes the coupling depend explicitly on E . This means that the free energy reads explicitly

$$\mathcal{F}_{\text{sc}} = \int \left[\left(a_0 - a_1 E \sum_j |\nabla \psi_j|^2 \right) |\Phi|^2 + b_s |\nabla \Phi|^2 + c_s |\Phi|^4 \right] d\mathbf{r}, \quad (\text{S15})$$

where the constants are chosen as above, $a_0 = 10t + 60$, $b_s = c_s = 1$, except that $a_1 = 500$ now. In this case, the effect of the lock-in energy E appears both explicitly, as a prefactor to the interaction, and implicitly, through its effect on $\psi_j(\mathbf{r})$. It should be noted that, the value of a_1 here is an exaggerated one, which is chosen to show more clearly the effect of enhancement of SC order by CDW fluctuation. Actually, the position of SC dome can be tuned by changing the value of it, which will be discussed later.

S10. ON THE COUPLING BETWEEN SUPERCONDUCTIVITY AND CDW FLUCTUATIONS

McMillan analyzed the collective modes of the discommensuration (DC) network near the commensurate-incommensurate transition in the NC regime; he considered only the phase fluctuations, approximating the amplitude as constant². He had previously found that, near the transition, DCs form a spatially separated “lattice” structure⁴. The fact that this DC network is stable in the NC regime of the phase diagram implies that its low energy excitations are phonons of that emergent lattice. From the equation of motion of the small-phase fluctuations on top of the DC periodic configuration, two types of collective vibrational modes were found: a gapless mode corresponding to the collective motion of DC lattice and a gapped “phason” mode. In other words, whereas in a uniformly incommensurate state phasons are linearly dispersing gapless modes, the smaller Brillouin zone imposed by the DC superlattice in the NC regime causes the “folding” and gapping of the phase excitations that hence split into two branches.

The coupling between CDW and SC in our G-L theory is motivated precisely by this observation. Since the DCs form a periodic structure and the onset of SC correlates with the loss of commensurability across a number of transition metal dichalcogenides, it is natural to speculate that the new phonons of this emergent lattice play a role in mediating an attractive interaction between electrons ultimately leading to superconducting pairing.

Such coupling is embodied in our SC free energy of Eq. (3) in the main text. Note however that one has to generically consider both the phase, $\theta_j(\mathbf{r})$, and amplitude, $\varphi_j(\mathbf{r})$, fluctuations of the CDW order parameter²⁴, $\psi_j(\mathbf{r}) = \varphi_j(\mathbf{r})e^{i\theta_j(\mathbf{r})}$, and our approach takes those two into account naturally (see Figs. 2b and 2c). Therefore, our theory should couple both amplitude and phase fluctuation modes to the SC order parameter $\Phi(\mathbf{r})$. Their minimal coupling via $-a_1 \sum_j |\nabla \psi_j|^2 |\Phi(\mathbf{r})|^2$ that we introduce in Eq. 2 ensures precisely that both *phason* and *amplitudon* modes couple to the SC order parameter, and the negative sign reflects the phenomenological assumption (grounded on the experimental correlation between SC and the loss of commensurability), that these fluctuations promote SC pairing [i.e., the existence of fluctuations permits lowering the total free energy with the development of a non-zero superconducting order parameter].

S11. CHOICE OF THE SUPERCONDUCTING FREE ENERGY PARAMETERS

The key observation in relation to our modeling of the interplay between the CDW (ψ_j) and SC (Φ) order parameters is that, experimentally, $T_{sc} \ll T_{cdw}$. Since ARPES data has established that the CDW order parameter (excitonic gap) has a mean-field-like temperature dependence^{26,27}, the large experimental ratio $T_{cdw}/T_{sc} \sim 20$ tells us that the onset of SC takes place at temperatures where the CDW order parameter is already at or near its $T = 0$ saturation value (see, for example, supplementary Fig. S2). In addition, as mentioned in our main text, it is experimentally known that the CDW persists in the SC phase. These two facts suggest that, in a first approximation, the emergence of SC order can be studied neglecting the self-consistent feedback that the development of this new order parameter might have in the CDW stability.

Under these conditions, the solution of the SC order parameter can proceed as if the CDW DCs texture is an independent, “externally-imposed” modulation of the superconducting pairing potential. This defines our working assumption, and means that we have now to solve a relatively conventional Ginzburg-Landau superconductivity problem, except that the quadratic coefficient in \mathcal{F}_{sc} , a_s , is an explicit function of the position. Consequently, the parameters b_s and c_s have the usual meaning, and determine the magnitude of the order parameter in the usual way²⁸. More specifically:

1. The parameters b_s and c_s have no effect in the position of the SC phase boundary in the phase diagram. This is because the SC transition described by \mathcal{F}_{sc} is of second order and, consequently, the transition temperature is determined entirely by the change in sign of the quadratic coefficient, a_s .
2. As a result of the non-uniformity of a_s [via its dependence on $\nabla\psi_j(\mathbf{r})$], regions of space where $a_s < 0$ will be superconducting, while those with $a_s > 0$ are normal. This leads to the sequence of transitions described in the section “Ramifications” of the main text, from nucleation of 0-dimensional SC dots, to proliferation (percolation) into a 1-dimensional SC network, to overall 2D superconductivity with $\Phi(\mathbf{r})$ finite everywhere.
3. The only parameter in the SC free energy with a spatial dependence is a_s . Therefore, the actual value of c_s only determines the magnitude of $\Phi(\mathbf{r})$: the larger c_s is, the smaller the overall magnitude of $\Phi(\mathbf{r})$. Hence, the magnitude of c_s simply sets the scale of variation of $\Phi(\mathbf{r})$. (In practice, except when we need quantitative values of the free energy, one can always set $c_s = 1$, which corresponds to absorbing its actual magnitude by redefining the

scale of the free energy itself.)

4. The constant b_s determines the stiffness of $\Phi(\mathbf{r})$. The larger it is, the more that contribution in the free energy penalizes fast spatial variations of the SC order parameter (in a type II superconductor with homogeneous pairing potential, b_s controls the coherence length). If $b_s = 0$, the spatial profile of $\Phi(\mathbf{r})$ can follow precisely that of the DC network, where the localization length of $\Phi(\mathbf{r})$ coincides with the size of the DCs. In contrast, with a finite b_s , the localization length of $\Phi(\mathbf{r})$ will no longer be determined only by the size of the DC, but also by the magnitude of b_s itself which determines how tightly $\Phi(\mathbf{r})$ can be confined within a DC. In general, an increase in b_s translates into a decrease of T_{sc} in the NC regime due to the inhomogeneous nature of the superconducting phase in our model in this region of the phase diagram. Note, however, that although b_s controls how closely the spatial extent of $\Phi(\mathbf{r})$ follows that of a DC, it does not change the fact that DCs are essential for the nucleation of the superconducting order.

For the purpose of clarity and visibility of the different phases, the phase diagram shown in the main text has been obtained with $a_0 = 10t + 60$, $t = (T - T_{icdw})/10$, $a_1 = 500$. The ratio T_{cdw}/T_{sc} in that figure underestimates the actual experimental value ($T_{cdw}/T_{sc} = 20$). However, the experimental ratio can easily be matched by adjusting the coupling between SC and CDW fluctuations, a_1 . This is demonstrated explicitly in supplementary Fig. S3, where we show the effect of changing the magnitude of a_1 in the boundary of the SC dome. It is clear that the position of the T_{sc} line can be adjusted by reducing a_1 .

S12. SOLVING FOR THE EQUILIBRIUM SUPERCONDUCTING ORDER PARAMETER

We must determine the solution $\Phi(\mathbf{r})$ that minimizes the free energy \mathcal{F}_{sc} in either of the forms written in (S14) or (S15). For every point (E, t) in the parameter space of the phase diagram, we replace $\psi_j(\mathbf{r})$ by the corresponding equilibrium solution arising from the minimization of \mathcal{F}_{cdw} . Since $\psi_j(\mathbf{r})$ is non-uniform in space outside the C-CDW phase, this turns the equations (S14) and (S15) into non-uniform Ginzburg-Landau problems.

Numerically, we solve the Euler-Lagrange equations for $\Phi(\mathbf{r})$ using the CDW texture $(\sum_j |\nabla \psi_j(r)|^2)$ itself as the initial trial solution which is then relaxed under periodic boundary conditions consistent with the CDW and DC network.

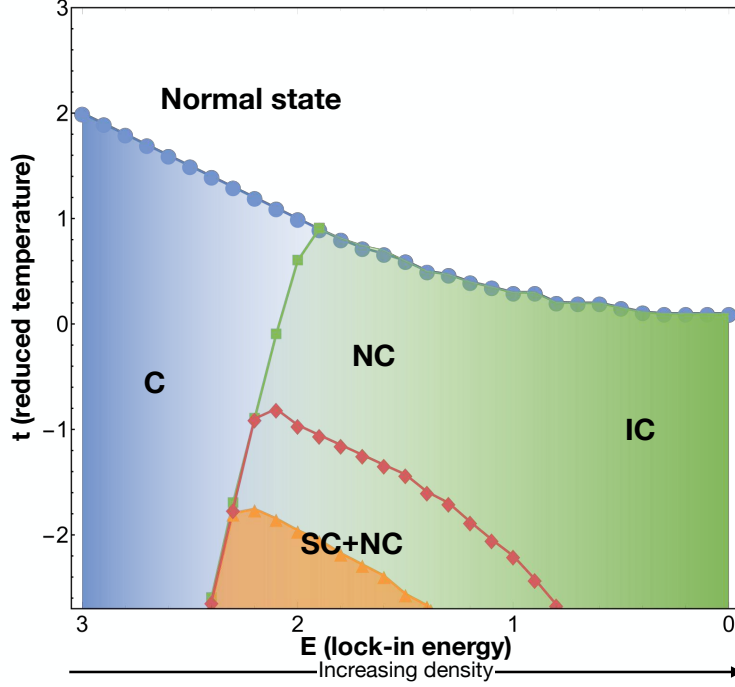
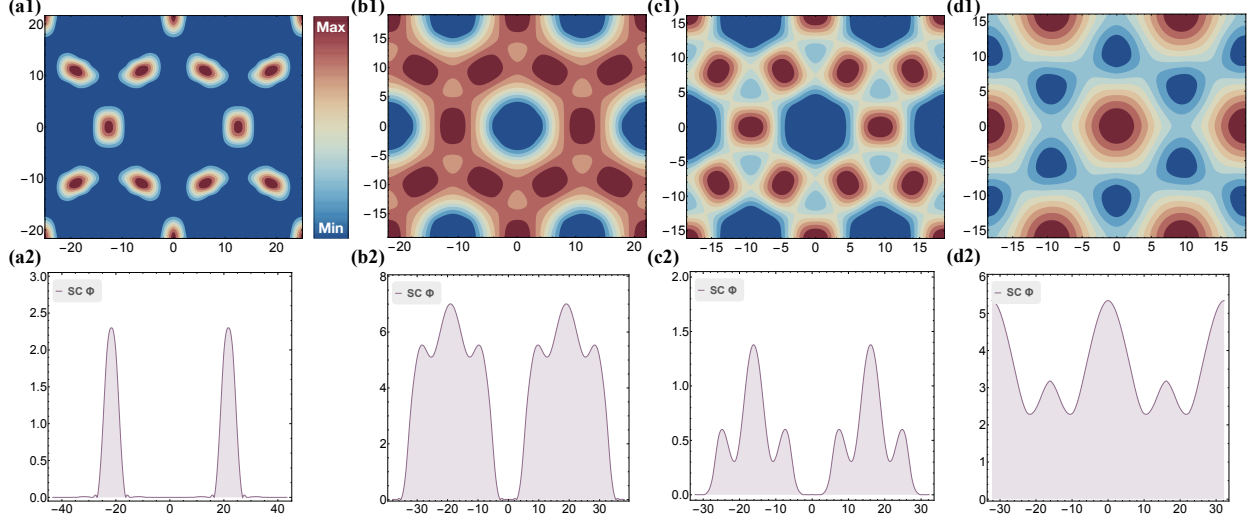


FIG. S3. Phase diagram of the G-L model emphasizing how the parameter a_1 in the superconducting free energy \mathcal{F}_{sc} determines the position of the SC phase boundary within the NC region. The red line is the same shown in Fig. 1 of the main text, and has been obtained with $a_1 = 500$. The orange line marks the same SC boundary, but obtained with a smaller value, $a_1 = 250$.

S13. REAL-SPACE SUPERCONDUCTING ORDER

Fig. S4 shows the real space SC order in different cases that correspond to the solutions that minimize the total free energy in different regions of the (E, t) parameter space. temperature right below the $T_{\text{sc}}^{(0)}$, isolated SC islands emerge at the intersection of three CDW DCs and forms a Kagome lattice, as shown in panel (a1-2). At very low temperature ($T < T_{\text{sc}}^{(2)}$), the area of SC network expands and is able to cover the entire space, a 2D SC regime is achieved. Due to the linear dependence on E in the CDW and SC coupling a_1 , when E decreases, the SC order gets suppressed so one can get the dome shape of SC phase as shown in the phase diagram from main text. If the E -dependence is removed, in the IC phase (with very small E), because of the strong fluctuation of CDW order parameter (relative to CCDW), it can still support a SC order, as shown in panel Fig. S4(d1-2).



-
- ¹ K. Nakanishi and H. Shiba, *J. Phys. Soc. Jpn.* **43**, 1839 (1977).
 - ² W. L. McMillan, *Phys. Rev. B* **16**, 4655 (1977).
 - ³ A. E. Jacobs and M. B. Walker, *Phys. Rev. B* **21**, 4132 (1980).
 - ⁴ W. L. McMillan, *Phys. Rev. B* **14**, 1496 (1976).
 - ⁵ D. E. Moncton, J. D. Axe, and F. J. Disalvo, *Phys. Rev. Lett.* **34**, 734 (1975).
 - ⁶ B. Sipos, A. F. Kusmartseva, A. Akrap, H. Berger, L. Forró, and E. Tutiš, *Nat. Mater.* **7**, 960 (2008).
 - ⁷ M. Leroux, I. Errea, M. Le Tacon, S.-M. Souliou, G. Garbarino, L. Cario, A. Bosak, F. Mauri, M. Calandra, and P. Rodière, *Phys. Rev. B* **92**, 140303 (2015).
 - ⁸ D. B. McWhan, R. M. Fleming, D. E. Moncton, and F. J. DiSalvo, *Phys. Rev. Lett.* **45**, 269 (1980).
 - ⁹ A. H. Castro Neto, *Phys. Rev. Lett.* **86**, 4382 (2001).
 - ¹⁰ W. L. McMillan, *Phys. Rev. B* **12**, 1187 (1975).
 - ¹¹ Y. I. Joe, X. M. Chen, P. Ghaemi, K. D. Finkelstein, G. a. de la Peña, Y. Gan, J. C. T. Lee, S. Yuan, J. Geck, G. J. MacDougall, T. C. Chiang, S. L. Cooper, E. Fradkin, and P. Abbamonte, *Nat. Phys.* **10**, 421 (2014), 1309.4051.
 - ¹² A. Kogar, G. A. de la Pena, S. Lee, Y. Fang, S. X.-L. Sun, D. B. Lioi, G. Karapetrov, K. D. Finkelstein, J. P. C. Ruff, P. Abbamonte, and S. Rosenkranz, *Phys. Rev. Lett.* **118**, 027002 (2017).
 - ¹³ L. J. Li, E. C. T. O’Farrell, K. P. Loh, G. Eda, B. Özyilmaz, and A. H. Castro Neto, *Nature* **529**, 185 EP (2015).
 - ¹⁴ A. M. Novello, M. Spera, A. Scarfato, A. Ubaldini, E. Giannini, D. R. Bowler, and C. Renner, *Phys. Rev. Lett.* **118**, 017002 (2017).
 - ¹⁵ S. Yan, D. Iai, E. Morosan, E. Fradkin, P. Abbamonte, and V. Madhavan, *Phys. Rev. Lett.* **118**, 106405 (2017).
 - ¹⁶ K. Nakanishi and H. Shiba, *J. Phys. Soc. Jpn.* **44**, 1465 (1978).
 - ¹⁷ P. A. Lee, T. M. Rice, and P. W. Anderson, *Solid State Commun.* **14**, 703 (1974).
 - ¹⁸ A. Kotani, *J. Phys. Soc. Jpn.* **42**, 408 (1977).
 - ¹⁹ A. Kotani, *J. Phys. Soc. Jpn.* **42**, 416 (1977).
 - ²⁰ See Supplemental Material at [URL will be inserted by publisher], which includes references^{1–28}.
 - ²¹ C. Chen, B. Singh, H. Lin, and V. M. Pereira, *Phys. Rev. Lett.* **121**, 226602 (2018).
 - ²² K. Nakanishi and H. Shiba, *J. Phys. Soc. Japan* **45**, 1147 (1978).
 - ²³ P. Bak and V. J. Emery, *Phys. Rev. Lett.* **36**, 978 (1976).
 - ²⁴ S. A. Jackson, P. A. Lee, and T. M. Rice, *Phys. Rev. B* **17**, 3611 (1978).
 - ²⁵ K. Nakanishi, H. Takater, Y. Yamada, and H. Shiba, *J. Phys. Soc. Jpn.* **43**, 1509 (1977).
 - ²⁶ C. Monney, E. F. Schwier, M. G. Garnier, N. Mariotti, C. Didiot, H. Cercellier, J. Marcus, H. Berger, A. N. Titov, H. Beck, and P. Aebi, *New J. Phys.* **12**, 125019 (2010).

- ²⁷ P. Chen, Y.-H. Chan, X.-Y. Fang, Y. Zhang, M.-Y. Chou, S.-K. Mo, Z. Hussain, A.-V. Fedorov, and T.-C. Chiang, [Nat. Commun. **6**, 8943 \(2015\)](#).
- ²⁸ M. Tinkham, *Introduction to Superconductivity: Second Edition* (McGraw Hill, Inc., New York, 1996).